Circumventing the polariton bottleneck via dark excitons in 2D semiconductors

Citation for the original published paper (version of record):
Fitzgerald, J., Rosati, R., de Amorim Ferreira, B. et al (2024). Circumventing the polariton bottleneck via dark excitons in 2D semiconductors. Optica, 11(9): 1346-1351.
http://dx.doi.org/10.1364/OPTICA.528699

(article starts on next page)

OPTICA

Circumventing the polariton bottleneck via dark excitons in 2D semiconductors

Jamie M. Fitzgerald,[1,*] Roberto Rosati,[1] Beatriz Ferreira,[2] Hangyong Shan,[3] Christian Schneider,[3] and Ermin Malic[1]

[1] Department of Physics, Philipps-Universität Marburg, 35032, Marburg, Germany
[2] Department of Physics, Chalmers University of Technology, 412 96, Gothenburg, Sweden
[3] Carl von Ossietzky Universität Oldenburg, Fakultät V, Institut für Physik, 26129 Oldenburg, Germany
*jamie.fitzgerald@physik.uni-marburg.de

Received 26 April 2024; revised 24 July 2024; accepted 24 July 2024; published 19 September 2024

Efficient scattering into the exciton polariton ground state is a key prerequisite for generating Bose–Einstein condensates and low-threshold polariton lasing. However, this can be challenging to achieve at low densities due to the polariton bottleneck effect that impedes phonon-driven scattering into low-momentum polariton states. The rich exciton landscape of transition metal dichalcogenides (TMDs) provides potential intervalley scattering pathways via dark excitons to rapidly populate these polaritons. Here, we present a theoretical and fully microscopic study exploring the time- and momentum-resolved relaxation of exciton polaritons supported by a $MoSe_2$ monolayer integrated within a Fabry–Perot cavity. By exploiting phonon-assisted transitions between momentum-dark excitons and the lower polariton branch, we demonstrate that it is possible to circumvent the bottleneck region and efficiently populate the polariton ground state. Furthermore, this intervalley pathway is predicted to give rise to, yet unobserved, angle-resolved phonon sidebands in low-temperature photoluminescence spectra that are associated with momentum-dark excitons. This represents a distinct signature for efficient phonon-mediated polariton-dark-exciton interactions.

https://doi.org/10.1364/OPTICA.528699

1. INTRODUCTION

Transition metal dichalcogenide (TMD) monolayers support tightly bound excitons with binding energies in the hundreds of meV [1,2]. Alongside optically accessible bright excitons [3], these 2D semiconductors also exhibit a rich variety of dark excitonic states. In particular, intervalley excitons, where the constituent electron and hole are located in different valleys of the hexagonal Brillouin zone, possess a large center-of-mass momentum that forbids direct radiative excitation and recombination [4]. These momentum-dark states can be efficiently populated via exciton-phonon scattering on a femtosecond timescale [5–8], meaning that the energetic ordering of the exciton landscape plays a crucial role in determining relaxation dynamics, photoluminescence (PL), and transport [9–11].

The combination of a large exciton binding energy and oscillator strength makes TMDs excellent candidates for room-temperature polaritonics [12–15]. Exciton polaritons are hybrid light-matter states that arise when an excitonic material is integrated within an optical cavity, and the light-exciton coupling strength exceeds all material and photonic dissipation channels [16,17]. Recently, exciton polariton condensation at cryogenic temperatures [18] and room-temperature polariton lasing [19,20] have been demonstrated for TMDs. These important milestones highlight the growing need to understand how exciton relaxation is modified for 2D semiconductors within the strong coupling regime over a wide range of temperatures. Alongside polariton-polariton [21] and polariton-electron [22] interactions, polariton-phonon scattering is one of the main mechanisms driving polariton relaxation, and even dominates at low densities. Previously, we have found that the substantial photonic character and greatly reduced density of states of the lower polariton (LP) branch within the lightcone drastically suppress acoustic-phonon-driven intravalley scattering in TMDs by two orders of magnitude [23], in line with earlier studies on conventional semiconductors [24,25]. Combined with the short radiative lifetime of polaritons, this leads to a severe reduction in emission at small angles and is known as the "polariton bottleneck effect" [24,25]. The bottleneck has significant implications for the performance of polariton-based lasing devices [26,27], as well as fundamental studies on polariton condensates [28]. In both cases, a mechanism is needed to populate the ground state at a faster rate than the radiative lifetime to achieve the required minimum polariton occupation. Vibrationally assisted polariton relaxation has been demonstrated to be an effective strategy to suppress the bottleneck effect at elevated temperatures. For organic semiconductors this tends to be particularly efficient due to a broad energetic range of available vibrational modes [29], while for inorganic [30,31] and crystalline hybrid semiconductors [32], the LP branch can be tuned such that the energy separation between its minimum and the bottleneck

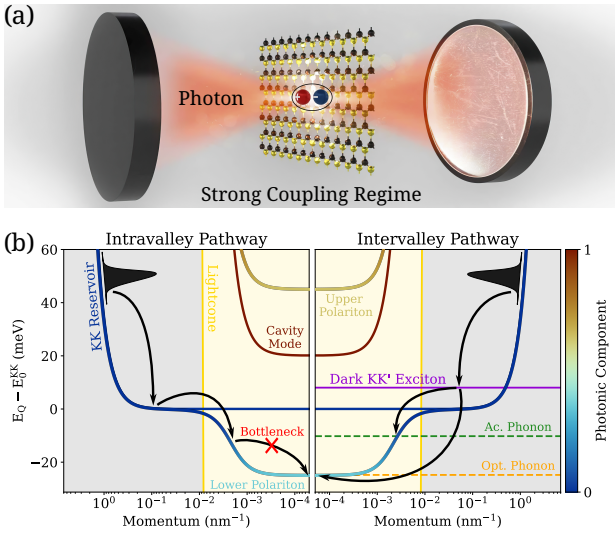

Fig. 1. (a) Illustration of a TMD monolayer integrated within a Fabry–Perot microcavity in the strong coupling regime. (b) Schematic of possible relaxation processes (black arrows) for the lower branch of a molybdenum-based exciton polariton. The left-hand side shows the bottleneck effect for intravalley scattering via acoustic phonons. The right-hand side shows the possible intervalley relaxation processes via acoustic (dashed green line) and optical (dashed orange line) phonon scattering from dark KK′ excitons (solid purple line). For this particular cavity detuning ($\Delta = 20$ meV), the $\vec{Q} = 0$ polariton state is exactly one optical phonon energy lower than the bottom of the KK′ valley.

reservoir coincides with the energy of an optical phonon. This strategy has been demonstrated to reduce the lasing threshold for a quantum well polariton laser [31]. Further approaches for boosting polariton relaxation involve using spatial confinement [33], and polariton-polariton scattering at higher densities [21,25].

The implications of the full exciton landscape in TMDs have yet to be understood in the context of exciton polariton relaxation. Recently, the important role of dark exciton states in TMD polaritonics was demonstrated by using the Rabi splitting to push the LP below a dark excitonic state in a WSe_2 monolayer, leading to a brightening of PL via the increased occupation of the LP branch [34]. Furthermore, signatures of phonon-driven intervalley scattering between polaritons and momentum-dark excitons in WSe_2 were recently identified in reflection spectra [35]. Using a Wannier–Hopfield approach [36,37], we explore in this work how exciton polaritons supported by a $MoSe_2$ monolayer integrated within a Fabry–Perot microcavity relax towards the lightcone [Fig. 1(a)]. In particular, we highlight how phonon-assisted scattering from the momentum-dark exciton can bypass the bottleneck region and allow for the efficient population of low-momentum states in the LP branch at room temperature [Fig. 1(b)]. This leads to highly detuning-dependent and material-specific relaxation dynamics based on the energy separation of the LP branch and the dark excitons. Furthermore, we show that at low temperatures a unique, to-date unobserved, phonon sideband signature appears in PL. Distinct from the bare exciton case [10,38], these sidebands are angle-resolved and specific to molybdenum-based TMDs within the strong coupling regime. Lastly, in Supplement 1, we confirm the existence of a polariton bottleneck at low temperatures through a detuning-dependent PL experiment. Using our microscopic model, we provide evidence for its circumvention by phonon-driven intervalley scattering as the cavity is blue detuned.

2. RESULTS

A. Bypassing the Polariton Bottleneck

Detuning a microcavity via the cavity length [i.e., mirror separation; see Fig. 1(a)] modifies the dispersion and light-exciton composition of the LP branch within the lightcone [Fig. 1(b)]. This impacts both the strength of polariton-phonon scattering [23,39], and the relative position of bright and dark states within the energy landscape [34,40] (the latter are unmodified by the presence of the microcavity). As a result, significant control over the temporal evolution of the polariton population is gained. To explore this, we apply a material-specific Wannier–Hopfield method [36,37] to model exciton polaritons supported by an hBN-encapsulated $MoSe_2$ monolayer integrated in the center of a symmetric $\lambda/2$ Fabry–Perot cavity [Fig. 1(a)]. Trion-polaritons [41], as well as phonon-driven scattering between trions and polaritons [42], have been previously observed. In our work, we assume negligible doping, so that trion effects can be neglected. We consider only the lowest 1s excitons associated with the KK, KK′, and KΛ states, where the first and second letters denote the reciprocal-space valley in which the respective Coulomb-bound hole and electron are localized [4], respectively. Solving the Wannier equation reveals that $MoSe_2$ is a direct semiconductor, where the dark KK′ excitons [solid purple line in Fig. 1(b)] lie about 10 meV above the bottom of the bright KK exciton dispersion (E_0^{KK}, solid blue curve) [9]. In the context of bare exciton optics and dynamics, KK′ excitons in $MoSe_2$ monolayers play only a minor role: they lead to a small linewidth increase in linear optical spectra at elevated temperatures due to phonon absorption [5]. In stark contrast, within the strong coupling regime, KK′ excitons are surprisingly essential in determining the polariton occupation within the lightcone as they can provide an additional exciton reservoir via phonon-induced intervalley population transfer.

Due to their short radiative lifetime, a correct description of polariton thermalization requires time-resolved simulations. The dynamics of the incoherent polariton occupation of the nth branch, at the center-of-mass momentum $\vec{Q}$, is found to be governed by the momentum-dependent semiclassical Boltzmann equation [16]

$$\dot{N}_{n\vec{Q}}(t) = \sum_{m,\vec{Q}'} W_{m\vec{Q}',n\vec{Q}} N_{m\vec{Q}'}(t) - 2\tilde{\Gamma}^{\text{out}}_{n\vec{Q}} N_{n\vec{Q}}(t), \qquad (1)$$

where $\tilde{\Gamma}^{\text{out}}_{n\vec{Q}}$ is the total out-scattering rate, which is the sum of the polariton radiative decay, $\gamma_{n\vec{Q}}$, and the phonon dephasing rate $\Gamma_{n\vec{Q}}$. Furthermore, $W_{m\vec{Q}',n\vec{Q}}$ is the corresponding in-scattering matrix describing the rate of scattering from the state $|m,\vec{Q}'\rangle$ to $|n,\vec{Q}\rangle$ via both phonon absorption and emission. Crucially, we include the full momentum and valley dependence of the in- and out-scattering rates, allowing us to explore the role of the exciton landscape on polariton relaxation. We initialize all simulations with a Gaussian distribution centered at 50 meV in the LP branch to mimic non-resonant excitation [16,17]. Further details on the theoretical approach can be found in Supplement 1.

The steady-state momentum-resolved polariton occupation, $N_{\vec{Q}}(t_\infty)$, is shown in Fig. 2(a) for three representative detunings at room temperature. Outside of the lightcone ($Q = \omega/c$, denoted by the vertical gold line), the polaritons closely follow a thermalized Boltzmann distribution, $N^0_{\vec{Q}}$ (dashed lines), for all three detunings. We will refer to these purely excitonic states as the "KK exciton

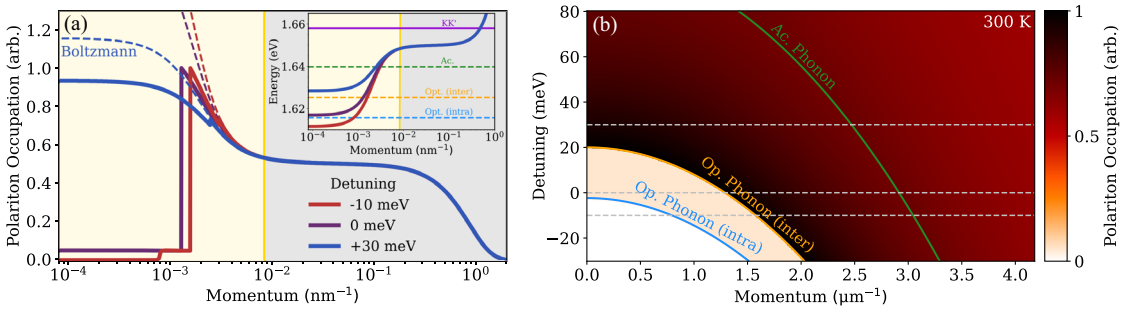

Fig. 2. (a) Lower polariton steady-state occupation for three representative detunings (defined at zero momentum, $E_0^{\mathrm{cav}} - E_0^{\mathrm{exc}}$) at a temperature of 300 K (solid lines), and the corresponding thermalized Boltzmann distributions (dashed lines). The inset shows the polariton dispersion for each detuning. (b) Detuning dependence of the steady-state polariton occupation within the lightcone. The orange and green lines show the opening of optical and acoustic phonon scattering channels from the KK′ exciton valley, respectively. This corresponds to a phonon energy below the bottom of the KK′ exciton dispersion. The blue line shows the opening of the intravalley optical phonon channel, while the three horizontal lines indicate the detunings considered in Fig. 2(a).

reservoir" [see Fig. 1(b)]. In contrast, the steady-state occupation within the lightcone is strongly detuning-dependent. It can be expressed as

$$N_{n\vec{Q}}(t_\infty) = \frac{\Gamma_{n\vec{Q}}}{\Gamma_{n\vec{Q}} + \gamma_{n\vec{Q}}} N^0_{n\vec{Q}}\,, \tag{2}$$

which can be derived from the static limit of Eq. (1) assuming that the in-scattering is dominated from states outside the lightcone (see Supplement 1). The prefactor quantifies the ratio of polaritons that are scattered back into the exciton reservoir to be recycled, relative to the total out-scattering rate. The latter includes polaritons that escape from the cavity via mirror leakage. While both the phonon-driven out-scattering and radiative decay rate are sensitive to the tunable exciton-light composition, the former also crucially depends on the available scattering channels that are allowed by energy-momentum conservation.

For a red-detuned cavity ($\Delta = E_0^{\mathrm{cav}} - E_0^{\mathrm{exc}} = -10$ meV, red line), the LP at low momenta within the lightcone is more photon-like [i.e., a sharper dispersion; see red curve in the inset of Fig. 2(a)] and possesses a negligible occupation. This exemplifies the bottleneck effect and highlights the reluctance of polaritons to thermalize in the absence of strong scattering channels, i.e., there is a large deviation between the calculated steady-state occupation and a Boltzmann distribution [red solid versus dashed line in Fig. 2(a)] due to the suppression of intravalley acoustic phonon scattering within the lightcone [23]. For increasing momenta within the lightcone, the occupation shows three sharp step-like increases before tending towards the Boltzmann distribution. This is indicative of the opening of specific phonon scattering channels [40]. The first small jump in occupation at around 8×10^{-4} nm^{-1} is the opening of the intravalley optical phonon scattering channel. Above this particular momentum, the energy-momentum conservation can be fulfilled and optical phonons (with an energy of 34 meV [43]) can scatter from the KK exciton reservoir into the lightcone [30,31]. The other two sharp jumps are a consequence of the opening of intervalley scattering channels from the KK′ exciton reservoir via optical (33 meV) and acoustic (18 meV) K phonons [43] at $Q = 1.6 \times 10^{-3}$ and 3×10^{-3} nm^{-1}, respectively. In particular, the larger jump in occupation stems from the optical phonon-driven intervalley scattering.

At zero detuning [$\Delta = 0$, purple line in Fig. 2(a)], there is a small increase in occupation at $\vec{Q} = 0$ as the intravalley optical phonon channel is now open over all possible LP momenta within the lightcone (i.e., the purple dispersion is above the dashed blue line in the inset), but there is still a substantially depleted population compared to the thermalized limit (purple dashed line). The two step-like increases from intervalley scattering are still present, but slightly shifted towards lower momenta due to the shallower polariton dispersion (purple curve, inset). The occupation within the lightcone changes drastically in a blue-detuned cavity ($\Delta = +30$ meV, blue line). There is now only one small step-like increase due to the opening of the acoustic phonon channel, and the occupation follows a slightly depleted Boltzmann distribution within the lightcone. This is because optical phonon-driven scattering from KK′ excitons is now possible at all momenta (see blue curve, inset), revealing that momentum-dark excitons can act as an additional reservoir to efficiently populate the entire LP branch at elevated temperatures.

These observations cannot be explained by the detuning-induced change in the light-exciton nature of the polariton (i.e., Hopfield coefficients), as the changes in the population are very sharp in momentum. To further illustrate this point, in Fig. 2(b) we show the steady-state LP occupation against momentum and detuning within the lightcone. There are three distinct regions, which are separated by the opening of intra- (blue line) and intervalley (orange line) optical phonon scattering channels, as well as the opening of the intervalley acoustic channel (green line). The momentum at which the energy-momentum conservation can be satisfied for an intervalley scattering process towards the LP depends on the detuning, exciton reservoir energy, and the associated phonon energy. In the case of the KK′ exciton reservoir, this can be stated as $E_Q^{\mathrm{P}}(\Delta) = E_Q^{\mathrm{KK'}} - E^{\mathrm{ph}}$. Efficient population of the $\vec{Q} = 0$ state via the KK′ exciton reservoir is activated for a blue-detuned cavity of 20 meV. This occurs when the lowest LP state coincides in energy with the bottom of the KK′ valley minus the optical phonon energy [see schematic Fig. 1(b)]. In Supplement 1 we present a detuning study where all intervalley channels are artificially switched off. There, we find a severely reduced occupation within the lightcone at all detuning values, underlining the importance of these channels for bypassing the polariton bottleneck.

We have also performed low-temperature (3.5 K) and detuning-dependent PL experiments for an hBN-encapsulated $MoSe_2$ monolayer in an open cavity [44]. By varying the cavity length, the

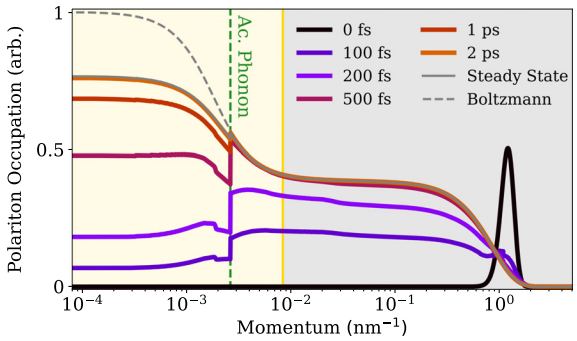

Fig. 3. Snapshots at fixed times of the lower polariton occupation at 300 K and a cavity detuning of $\Delta = 20$ meV. This particular detuning corresponds to the opening of the optical intervalley scattering channel for the polariton ground state.

PL intensity can be measured for different detunings. We find a clear indication of a relaxation bottleneck at negative detunings, reflected by a low PL. By increasing towards the zero and blue detuning regime, we observe a significant increase in the intensity, indicating the opening of relaxation channels and population of the low-momenta polariton states. By comparing to our microscopic model, we are able to describe this qualitative trend, and attribute the rise in PL intensity to the increased efficiency of acoustic K phonon-driven scattering from the dark KK′ exciton reservoir. See Supplement 1 for further details.

B. Time-Resolved Occupation

The solution of the polaritonic Boltzmann equation provides microscopic access to the temporal evolution of polariton states. Figure 3 illustrates the dynamics of the momentum-resolved LP occupation for a cavity detuned to $\Delta = 20$ meV, which corresponds to the opening of the optical phonon scattering channel [cf. Fig. 1(b)]. The KK reservoir outside the lightcone thermalizes within approximately 500 fs (solid and dashed gray lines coincide) via the efficient phonon-assisted scattering at room temperature, in agreement with previous studies of bare excitons in $MoSe_2$ [9]. This highlights that the dynamics outside of the lightcone can be understood with a purely excitonic picture. States within the lightcone that can be populated via both acoustic and optical phonon-driven scattering from the KK′ reservoir thermalize on a similar timescale as the KK exciton reservoir. In contrast, the low-momenta polaritons within the lightcone reach a steady-state [solid gray line given by the solution of Eq. (2)] on a longer timescale of about two ps. Interestingly, there is a significant rise in the polariton population already within 100 fs, which could have relevance for ultrafast polaritonic devices [27]. The crossover between these two regions of the LP dispersion is indicated by the large kink (vertical dashed green line) in the occupation. The size of this jump decreases over time as the occupation tends towards the quasi-thermalized limit of a depleted Boltzmann distribution.

The rapid build-up of occupation in the LP ground state is a direct consequence of the quick transfer of population from the initially populated KK exciton reservoir to KK′ excitons over tens of fs via phonon emission (see Supplement 1 for the dynamics of KK′ excitons). Given the elevated temperature and close energetic separation (<10 meV) between the KK and KK′ exciton reservoirs, the latter hold nearly half the total population at steady-state. Significantly, the large occupation of the KK′ exciton at high temperatures is not of a transient nature and does not depend on specific excitation conditions. This means it can act as an efficient exciton reservoir for the low-momenta LP states over tens or hundreds of ps. Overall, our results highlight that the dynamics of the LP branch can be divided into two domains. States outside the lightcone thermalize rapidly and independently of whether the system is in the strong coupling regime. In contrast, the states within the lightcone are predominately populated via a phonon-assisted in-scattering from the thermalized exciton reservoirs. Depending on the cavity detuning, this can efficiently bypass the bottleneck region and populate low-momenta polariton states.

C. Phonon-Assisted Polariton Photoluminescence

At low temperatures, phonon-assisted relaxation at all detunings is inefficient as the polariton radiative decay is larger than the total in-scattering rate [see Eq. (2)]. Because polaritons do not thermalize within the lightcone, scattering pathways from the KK′ reservoir imprint a distinctive signature on angle- and time-resolved *resonant* PL, i.e., evaluated at the polariton energy. This is shown in Fig. 4 for a zero-detuned system at 40 K. The resonant polariton PL can be expressed as (see Supplement 1):

$$I^{\mathrm{res}}_{n\vec{Q}}(t) = \frac{2\gamma_{n\vec{Q}}}{\gamma_{n\vec{Q}} + \Gamma_{n\vec{Q}}} N_{n\vec{Q}}(t), \tag{3}$$

where the prefactor quantifies the momentum-dependent ratio of the photon leakage rate out of the cavity and the total out-scattering. Note that there is a direct correspondence between the polariton in-plane momentum and the angle of PL emission, $\sin(\theta) = \hbar c Q / E^{\mathrm{P}}_{Q}$. We find an enhanced PL at emission angles corresponding to the opening of phonon scattering channels (dashed vertical lines in Fig. 4). Given the low temperature, the peaks at 10° and 20° are of a transient nature in the time range shown here. They grow in amplitude before peaking around 10–20 ps, and then slowly decay towards the steady state. This is a consequence of the KK′ exciton valley being initially overpopulated via intervalley transfer from the KK exciton reservoir, before then slowly thermalizing over tens of ps. The difference in PL peak height stems from the occupation, and is a consequence of a larger acoustic exciton-phonon matrix element and the increased excitonic character of the LP at larger momenta. The asymmetric lineshape with a long decaying tail is reminiscent of phonon-assisted PL, and is related to the kinetic energy distribution of the source exciton reservoir [45].

In tungsten-based TMDs, momentum-indirect excitons are energetically lower than the bright KK exciton and therefore carry the majority of the excitonic population at low temperatures. This large occupation results in pronounced phonon sidebands red-shifted by the phonon energy from the dark exciton energy [10,38]. These sidebands correspond to a weak momentum-conserving process where a momentum-indirect exciton can recombine and emit a virtual photon within the lightcone via the simultaneous interaction with a phonon. Here, we observe a similar process, but with the virtual photon replaced with a polariton state. This has two major consequences: (i) the mechanism is more efficient as it is now a resonant process with a real final state; (ii) while the usual phonon-assisted PL lineshape appears as a function of frequency, here it corresponds to the resonant PL evaluated along the LP dispersion [Eq. (3)]. This means it must be resolved with respect to the angle of emission, which can be shifted with

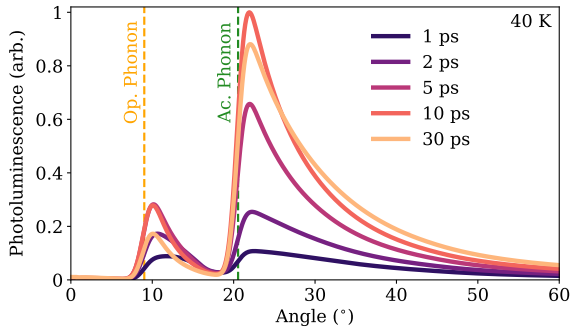

Fig. 4. Snapshots of the angle-resolved photoluminescence (PL) at a temperature of 40 K for a zero-detuned cavity. The PL is evaluated at the polariton energy along the lower branch dispersion. An integration over a 2° detection window is performed to mimic realistic experimental measurements.

cavity detuning (see Supplement 1 for a detuning study of the LP occupation at 40 K). These angle-dependent PL peaks represent a new hallmark of polariton-phonon interactions. To date, only a Purcell enhancement of phonon sidebands has been predicted in cavity systems [46]. Note that this phonon-assisted polariton PL is contingent on the dark exciton energy being on the order of the exciton-light coupling strength above the bright exciton energy. This is satisfied for KK' excitons in molybdenum-based TMDs. In contrast, this process will be challenging to observe with a tungsten-based TMD as tuning the polariton to typical phonon energies below the KK′ or KΛ excitons will lead to extremely light-like polaritons. This is in stark contrast to the bare excitonic case where phonon sidebands are only visible in tungsten-based TMDs [10]. These findings offer promise in utilizing strong coupling physics as a probe of phonon-driven intervalley transitions.

3. CONCLUSION

In conclusion, we have demonstrated the crucial importance of the full exciton landscape, including dark and bright states, for polariton relaxation dynamics in TMD monolayers. At room temperature, we have shown that momentum-dark excitons can provide an efficient reservoir to populate the ground state and bypass the polariton bottleneck. At low temperatures, they lead to unique phonon sidebands visible in angle-resolved PL that can be controlled by cavity detuning. These signatures in the polariton PL provide an experimental tool to study the strength of intervalley polariton-phonon scattering, and potentially even measure the energy of momentum-dark excitons. Overall, our work provides microscopic insights into polariton dynamics in atomically thin semiconductors, and has technological relevance for the design of compact and low-threshold polariton lasers that operate at room temperature.

Funding. Ministry of Research and Culture (MWK) of Lower Saxony (Dynano); Deutsche Forschungsgemeinschaft (SFB 1083 and project 524612380).

Acknowledgment. The Marburg authors acknowledge funding from the DFG via SFB 1083 and the regular project 524612380, while the Oldenburg authors acknowledge funding by the MWK. Open access funding provided by the Open Access Publishing Fund of Philipps-Universität Marburg.

Disclosures. The authors declare no conflicts of interest.

Data availability. Data underlying the results presented in this paper are not publicly available at this time but may be obtained from the authors upon reasonable request.

Supplemental document. See Supplement 1 for supporting content.

REFERENCES

1. G. Wang, A. Chernikov, M. M. Glazov, *et al.*, "Colloquium: excitons in atomically thin transition metal dichalcogenides," Rev. Mod. Phys. **90**, 021001 (2018).
2. R. Perea-Causin, D. Erkensten, J. M. Fitzgerald, *et al.*, "Exciton optics, dynamics, and transport in atomically thin semiconductors," APL Mater. **10**, 100701 (2022).
3. A. Chernikov, T. C. Berkelbach, H. M. Hill, *et al.*, "Exciton binding energy and nonhydrogenic Rydberg series in monolayer WS2," Phys. Rev. Lett. **113**, 076802 (2014).
4. E. Malic, M. Selig, M. Feierabend, *et al.*, "Dark excitons in transition metal dichalcogenides," Phys. Rev. Mater. **2**, 014002 (2018).
5. M. Selig, G. Berghäuser, A. Raja, *et al.*, "Excitonic linewidth and coherence lifetime in monolayer transition metal dichalcogenides," Nat. Commun. **7**, 13279 (2016).
6. S. Brem, J. Zipfel, M. Selig, *et al.*, "Intrinsic lifetime of higher excitonic states in tungsten diselenide monolayers," Nanoscale **11**, 12381–12387 (2019).
7. D. Schmitt, J. P. Bange, W. Bennecke, *et al.*, "Formation of moiré interlayer excitons in space and time," Nature **608**, 499–503 (2022).
8. S. Bae, K. Matsumoto, H. Raebiger, *et al.*, "K-point longitudinal acoustic phonons are responsible for ultrafast intervalley scattering in monolayer MoSe2," Nat. Commun. **13**, 4279 (2022).
9. M. Selig, G. Berghäuser, M. Richter, *et al.*, "Dark and bright exciton formation, thermalization, and photoluminescence in monolayer transition metal dichalcogenides," 2D Materials **5**, 035017 (2018).
10. S. Brem, A. Ekman, D. Christiansen, *et al.*, "Phonon-assisted photoluminescence from indirect excitons in monolayers of transition-metal dichalcogenides," Nano Lett. **20**, 2849–2856 (2020).
11. R. Rosati, R. Schmidt, and S. Brem, "Dark exciton anti-funneling in atomically thin semiconductors," Nat. Commun. **12**, 7221 (2021).
12. S. Dufferwiel, S. Schwarz, F. Withers, *et al.*, "Exciton-polaritons in van der Waals heterostructures embedded in tunable microcavities," Nat. Commun. **6**, 8579 (2015).
13. L. Zhang, R. Gogna, W. Burg, *et al.*, "Photonic-crystal exciton-polaritons in monolayer semiconductors," Nat. Commun. **9**, 713 (2018).
14. S. Latini, E. Ronca, U. De Giovannini, *et al.*, "Cavity control of excitons in two-dimensional materials," Nano Lett. **19**, 3473–3479 (2019).
15. J. Zhao, A. Fieramosca, K. Dini, *et al.*, "Exciton polariton interactions in van der waals superlattices at room temperature," Nat. Commun. **14**, 1512 (2023).
16. V. Savona, C. Piermarocchi, A. Quattropani, *et al.*, "Optical properties of microcavity polaritons," Phase Transit. **68**, 169–279 (1999).
17. A. Kavokin and G. Malpuech, *Thin Films and Nanostuctures: Cavity Polaritons* (Elsevier, 2003).
18. C. Anton-Solanas, M. Waldherr, M. Klaas, *et al.*, "Bosonic condensation of exciton-polaritons in an atomically thin crystal," Nat. Mater. **20**, 1233–1239 (2021).
19. J. Zhao, R. Su, A. Fieramosca, *et al.*, "Ultralow threshold polariton condensate in a monolayer semiconductor microcavity at room temperature," Nano Lett. **21**, 3331–3339 (2021).
20. H. Shan, L. Lackner, B. Han, *et al.*, "Spatial coherence of room-temperature monolayer WSe2 exciton-polaritons in a trap," Nat. Commun. **12**, 6406 (2021).
21. J. Zhao, A. Fieramosca, R. Bao, *et al.*, "Nonlinear polariton parametric emission in an atomically thin semiconductor based microcavity," Nat. Nanotechnol. **17**, 396–402 (2022).
22. V. Hartwell and D. Snoke, "Numerical simulations of the polariton kinetic energy distribution in GaAs quantum-well microcavity structures," Phys. Rev. B **82**, 075307 (2010).
23. B. Ferreira, R. Rosati, and E. Malic, "Microscopic modeling of exciton-polariton diffusion coefficients in atomically thin semiconductors," Phys. Rev. Mater. **6**, 034008 (2022).
24. F. Tassone, C. Piermarocchi, V. Savona, *et al.*, "Bottleneck effects in the relaxation and photoluminescence of microcavity polaritons," Phys. Rev. B **56**, 7554 (1997).

25. A. Tartakovskii, M. Emam-Ismail, R. Stevenson, *et al.*, "Relaxation bottleneck and its suppression in semiconductor microcavities," Phys. Rev. B **62**, R2283 (2000).
26. A. Imamog, R. Ram, S. Pau, *et al.*, "Nonequilibrium condensates and lasers without inversion: exciton-polariton lasers," Phys. Rev. A **53**, 4250 (1996).
27. T. Liew, I. Shelykh, and G. Malpuech, "Polaritonic devices," Phys. E **43**, 1543–1568 (2011).
28. H. Deng, H. Haug, and Y. Yamamoto, "Exciton-polariton Bose-Einstein condensation," Rev. Mod. Phys. **82**, 1489 (2010).
29. D. M. Coles, P. Michetti, C. Clark, *et al.*, "Vibrationally assisted polariton-relaxation processes in strongly coupled organic-semiconductor microcavities," Adv. Funct. Mater. **21**, 3691–3696 (2011).
30. F. Boeuf, R. André, R. Romestain, *et al.*, "Evidence of polariton stimulation in semiconductor microcavities," Phys. Rev. B **62**, R2279 (2000).
31. M. Maragkou, A. Grundy, T. Ostatnický, *et al.*, "Longitudinal optical phonon assisted polariton laser," Appl. Phys. Lett. **97**, 111110 (2010).
32. M. Laitz, A. E. Kaplan, J. Deschamps, *et al.*, "Uncovering temperature-dependent exciton-polariton relaxation mechanisms in hybrid organic-inorganic perovskites," Nat. Commun. **14**, 2426 (2023).
33. T. Paraïso, D. Sarchi, G. Nardin, *et al.*, "Enhancement of microcavity polariton relaxation under confinement," Phys. Rev. B **79**, 045319 (2009).
34. H. Shan, I. Iorsh, B. Han, *et al.*, "Brightening of a dark monolayer semiconductor via strong light-matter coupling in a cavity," Nat. Commun. **13**, 3001 (2022).
35. B. Ferreira, H. Shan, R. Rosati, *et al.*, "Revealing dark exciton signatures in polariton spectra of 2d materials," ACS Photonics **11**, 2215–2220 (2024).
36. J. M. Fitzgerald, J. J. P. Thompson, and E. Malic, "Twist angle tuning of moiré exciton polaritons in van der Waals heterostructures," Nano Lett. **22**, 4468–4474 (2022).
37. J. K. König, J. M. Fitzgerald, J. Hagel, *et al.*, "Interlayer exciton polaritons in homobilayers of transition metal dichalcogenides," 2D Materials **10**, 025019 (2023).
38. R. Rosati, K. Wagner, S. Brem, *et al.*, "Temporal evolution of low-temperature phonon sidebands in transition metal dichalcogenides," ACS Photonics **7**, 2756–2764 (2020).
39. F. Lengers, T. Kuhn, and D. E. Reiter, "Phonon signatures in spectra of exciton polaritons in transition metal dichalcogenides," Phys. Rev. B **104**, L241301 (2021).
40. B. Ferreira, R. Rosati, J. M. Fitzgerald, *et al.*, "Signatures of dark excitons in exciton-polariton optics of transition metal dichalcogenides," 2D Materials **10**, 015012 (2022).
41. N. Lundt, P. Nagler, A. Nalitov, *et al.*, "Valley polarized relaxation and upconversion luminescence from Tamm-plasmon trion-polaritons with a MoSe2 monolayer," 2D Materials **4**, 025096 (2017).
42. J. Jadczak, J. Debus, J. Olejnik, *et al.*, "Biexciton and singlet trion upconvert exciton photoluminescence in a MoSe2 monolayer supported by acoustic and optical *k*-valley phonons," J. Phys. Chem. Lett. **14**, 8702–8708 (2023).
43. Z. Jin, X. Li, J. T. Mullen, *et al.*, "Intrinsic transport properties of electrons and holes in monolayer transition-metal dichalcogenides," Phys. Rev. B **90**, 045422 (2014).
44. J.-C. Drawer, V. N. Mitryakhin, H. Shan, *et al.*, "Monolayer-based single-photon source in a liquid-helium-free open cavity featuring 65% brightness and quantum coherence," Nano Lett. **23**, 8683–8689 (2023).
45. D. Snoke, J. Wolfe, and A. Mysyrowicz, "Quantum saturation of a Bose gas: excitons in Cu2O," Phys. Rev. Lett. **59**, 827 (1987).
46. C. Böttge, M. Kira, and S. Koch, "Enhancement of the phonon-sideband luminescence in semiconductor microcavities," Phys. Rev. B **85**, 094301 (2012).